Methionine Uptake by Tumor Tissue: A Microautoradiographic Comparison with FDG

Roko Kubota, Kazuo Kubota, Susumu Yamada, Masao Tada, Toshihiro Takahashi, Ren Iwata and Nobuaki Tamahashi

Departments of Nuclear Medicine, Radiology and Pharmacology, Institute for Aging, Development and Cancer; Cyclotron and Radioisotope Center; Tohoku University and Clusterecore Institute of Biology, Sendai, Japan

L-methyl-^{11}C-methionine (^{11}C-Met) and 2-deoxy-2-^{18}F-fluoro-D-glucose (^{18}F-FDG) are used for tumor diagnosis and treatment evaluation by PET. In order to examine the role of these tracers in cancer imaging, intratumoral properties of ^{14}C-Met were studied and compared to those of ^{18}F-FDG. **Methods:** The distribution of ^{14}C-Met in various cellular elements of two different mouse malignant tumor tissues, MH134 and FM3A, was analyzed serially using microautoradiography within a period of 120 min after injection of the tracer. **Results:** Carbon-14-Met and ^{18}F-FDG showed different distributions in tumor tissue. Carbon-14-Met uptake by the tumor was mostly by viable cancer cells. The uptake by macrophages and other cellular components was low. The uptake was higher in the highly proliferative tumor but did not reflect protein synthesis. The rapid and slow growing tumors demonstrated that ^{14}C-Met uptake ratio was lower than that of ^{18}F-FDG, reflecting de novo DNA synthesis ratio. **Conclusion:** Carbon-14-Met uptake represents the presence of viable cancer cells. Carbon-11-Met may be suitable for treatment evaluation of individual tumors but not growth rates of different tumors. Flourine-18-FDG reflects tumor-host immune system reaction and is an excellent tool for pretreatment evaluation of tumors and determination of tumor proliferative activity.

Key Words: cancer imaging; methionine uptake; FDG; malignancy

J Nucl Med 1995; 36:484–492

L-Methyl-^{11}C-methionine (^{11}C-Met) and 2-deoxy-2-^{18}F-fluoro-D-glucose (^{18}F-FDG) are used for tumor diagnosis and evaluation of treatment effects by PET (*1–7*). Accumulation of ^{11}C-Met into malignant tissue is thought to be due to amino acid metabolism of cancer cells such as increased active transport and incorporation of amino acid into protein fractions (*8,9*). Carbon-11-Met is also incorporated into the lipid fraction and nucleic acids by transmethylation via S-adenosyl-L-methionine (*8*). Recent studies have revealed that tissue accumulation of ^{11}C-Met reflects amino acid active transport rather than protein synthesis rate (*10*). However, whether such a process accounts for the entire PET image profile is still unclear. Since tumors consist of various neoplastic and non-neoplastic cellular elements, and ^{11}C-Met uptake may be regulated by their own mechanisms, any PET image visualizes the entire radioactivity in various cellular elements. This visualization occurs whether the tracer is actively or passively transported, or whether the intracellular tracer is freely pooled or incorporated into proteins and others.

We have recently reported different cellular accumulation of ^{18}F-FDG in malignant tissues using microautoradiography (*11,12*). Comparison of ^{11}C-Met and ^{18}F-FDG uptake by the same tumor models analyzed by the same technique may provide important information on intratumoral properties of each tracer. In the present study, we report a unique uptake and incorporated patterns of ^{14}C-Met, as a representative of ^{11}C-Met, by various cellular elements in mouse malignant tumor models of different growth rates. The rate of bound radioactivity was studied by measuring residual radioactivity after removal of freely diffusible labeled compounds. We also compared tissue distribution of ^{14}C-Met and ^{18}F-FDG, and discussed the role of these tracers in cancer imaging.

MATERIALS AND METHODS

Animal Models

The study protocol was approved by the Laboratory Animal Care and Use Committee of Tohoku University. C3H/He female mice (10-wk-old) were subcutaneously injected with a 0.1 ml suspension of 10^7 syngeneic FM3A mammary carcinoma cells and 10^6 syngeneic MH134 hepatoma cells, respectively, into the left and right thighs, as previously described (*12*). Tracer experiments were performed 10 days after tumor transplantation when the volume doubling time of the tumor was 1.3 and 4.9 days for MH134 and FM3A, respectively. The age and volume of both tumors were the same when the tracer study was performed. Mice were fasted for 12 hr before the experiment but were provided with water ad libitum. Triple-tracer tissue distribution study was performed after 4 hr of fasting.

Tissue Distribution Study

Twenty-eight mice bearing both FM3A and MH134 tumors were injected intravenously through the lateral tail vein with 1 μCi (37 kBq) of methyl-^{14}C-methionine (Amersham International plc, Buckinghamshire, UK) dissolved in 0.2 ml of saline and sacrificed

Received Mar. 18, 1994; revision accepted Aug. 8, 1994.

For correspondence or reprints contact: Kazuo Kubota, MD, Department of Nuclear Medicine and Radiology, Institute for Aging, Development and Cancer, Tohoku University, 4-1 Seiryo-cho, Aoba-ku, Sendai 980-77, Japan.

1, 5, 15, 30, 45, 60 or 120 min later. Tissue specimens were excised, trimmed into two pieces and weighed. The first specimen was processed for radioactivity measurement using a liquid scintillation counter (LSC) as described previously (*12,13*). The second specimen was immersed in 15 ml of a mixture of ethanol and acetic acid (EtOH/AcOH) (19:1, vol/vol) for 24 hr at 0°C and 15 ml of distilled water twice for 24 hr each in order to fix proteins and to extract protein-free diffusible radioactive compounds. Following dehydration with 15 ml each of 70% EtOH aq and EtOH, samples were processed for LSC counting to measure residual radioactivity. Tissue radioactivity was expressed as the differential uptake ratio (DUR) (*14*):

$$\text{DUR} = \frac{\text{tissue counts/tissue weight}}{\text{injected dose counts/body weight}}.$$

To identify the ^{14}C-Met-carrying compound in tumors after the extraction, a comparative study using a standard fractionation analysis was performed in 15 mice under the same experimental condition as described above. The mice were sacrificed 5, 30 and 60 min after injection of the tracer. Tumor specimens were excised, trimmed into three pieces and weighed. The first and second specimens were processed as described above. The third specimens, homogenized and radiolabeled acid-precipitable materials, were divided into four fractions (lipids, RNA, DNA and proteins) by the method of Ishiwata et al. (*15*). Their radioactivity was measured using LSC as described above.

Triple-tracer Tissue Distribution Study

Another ten mice bearing both FM3A and MH134 tumors were injected with a mixture of 20 μCi (740 kBq) of ^{18}F-FDG, 1 μCi (37 kBq) of ^{14}C-Met and 1 μCi (37 kBq) of 6-^{3}H-thymidine (^{3}H-Thd, Amersham International plc, Buckinghamshire, UK) dissolved in 0.2 ml of saline and sacrificed 30 and 60 min later. Tissue samples were excised, weighed and their radioactivity measured using an autogamma counter and LSC. The technique used for differential measurement of three nuclides has been described in detail previously (*13*).

Double-tracer Macroautoradiography

Three C3H/He mice bearing both FM3A and MH134 tumors were injected with a mixture of 200 μCi (7.4 MBq) of ^{18}F-FDG and 5 μCi (185 kBq) of ^{14}C-Met dissolved in 0.2 ml saline and sacrificed 1 hr later. Tumors were dissected and frozen (*11,12*). Several 3.5-μm thick sections were mounted on clean glass slides, air dried and placed in direct contact with ARG films (MARG ^{3}H-type, Konica, Tokyo, Japan) for 2 hr to produce ^{18}F-FDG images. Three days later sections were placed in contact with separate films for 12 days to produce ^{14}C-Met whole images. Sections were later fixed and freely diffusible radioactive compounds were extracted in EtOH/AcOH for 10 min, washed out in gently running water for 30 min and air dried. Sections were placed in contact with separate films for 12 days to produce ^{14}C-Met-residual radioactive images. Sections were stained with hematoxylin and eosin (H&E) after exposure.

Time-course Micro-autoradiography with ^{14}C-Met

Twenty-four mice bearing both FM3A and MH134 tumors were injected with 5 μCi (185 kBq) of ^{14}C-Met dissolved in 0.2-ml saline and sacrificed 1, 5, 15, 30, 45 or 60 min later. Tumors were quickly removed, cut into frozen sections and 3.5-μm thick sections were processed for microautoradiography (*11,12*) as ^{14}C-Met-whole samples. Contiguous 3.5-μm thick sections from the same frozen blocks were mounted on clean glass slides. The fixation, washing and air drying was performed as described above to prepare ^{14}C-Met-residual radioactive samples. Sections were later dipped in NTB2 emulsion at 40°C and dried. After exposure for 20 days, sections of both ^{14}C-Met-whole and -residual radioactive samples were developed, fixed and stained with H&E. Nonradioactive tumor sections were processed in a similar manner as chemographic controls. The number of silver grains in various tumor regions, selected at random, was counted under a transmitted light brightfield microscope using a micrometer.

The other continuous sections (5, 30, 60 min) mounted on clean glass slides were removed from the slides before and after fixation/washing. The radioactivity was counted using LSC and the percentage of residual radioactivity was compared with the results of fractionation analysis.

The film response to ^{14}C radioactivity and the relationship between microautoradiographic grain numbers and ^{14}C radioactivity were determined using a commercially available autoradiographic ^{14}C-micro-scale (RPA.504L, Amersham International plc, Buckinghamshire, UK), which was placed directly in contact with ARG films for 12 days and emulsion-coated slides for 20 days. The grain density was measured using a densitometer for films and a microscope for microautoradiograms in a similar manner as described above.

RESULTS

Labeled Materials after Extraction

Carbon-14-Met uptake in tumor tissues and sections before and after extraction was compared with the fractionation analysis of ^{14}C-Met metabolites (Table 1). The residual radioactivity in tissues after extraction and its percentage to whole radioactivity were almost equivalent to the total of those in proteins, lipids, alkaline-labile fraction containing RNA hydrolysates and acid-labile fraction containing DNA hydrolysates. The labeled materials in tissues after extraction was considered to be proteins, lipids, RNA and DNA. Radioactivity in each of these four fractions increased with time. The percentage of protein-bound radioactivity became higher with time up to 67.0% (MH134) and 65.8% (FM3A) of the total bound radioactivity in the four fractions. The percentage of residual radioactivity after the treatment was comparable in tissues and in sections. Thus, the labeled materials in sections after fixation/extraction was also considered to be proteins, lipids, RNA and DNA as the same as those in tissues. Based on these findings, we defined the residual radioactivity in tumor tissue and section in this study as the ^{14}C-Met-acid precipitable fraction (APF) bound uptake.

Double-Tracer Macroautoradiograms and Microautoradiograms

Figure 1 shows typical macroautoradiograms of a section from MH134 and FM3A tumors 1 hr after injection of a mixture of ^{18}F-FDG and ^{14}C-Met. Macroautoradiograms of ^{14}C-Met-whole and -APF bound showed a similar heterogeneous distribution in both tumors. Fluorine-18-FDG distribution profile was more heterogeneous and different from both ^{14}C-Met profiles. The grain density was higher in MH134 than in FM3A in all macroautoradiograms. The

TABLE 1
Comparison of Residual Radioactivity in Tumors by the Extraction Method and by Fractionation Analysis of ^{14}C-Met in Tumors

A. Extraction (tissue and section)						
	Time after injection (min), DUR					
	5		30		60	
	MH134	FM3A	MH134	FM3A	MH134	FM3A
Tissue						
Whole	1.55 ± 0.13	1.26 ± 0.04	2.16 ± 0.09	1.71 ± 0.25	2.04 ± 0.25	1.66 ± 0.03
Residual	0.16 ± 0.07	0.16 ± 0.04	0.67 ± 0.21	0.51 ± 0.09	0.92 ± 0.15	0.75 ± 0.06
Residual/Whole	10.3%	12.7%	31.0%	29.8%	45.1%	45.2%
Section						
Residual/Whole	10.8 ± 1.6%	11.0 ± 1.5%	32.6 ± 2.7%	28.7 ± 1.8%	46.4 ± 1.2%	43.7 ± 1.6%

B. Fractionation analysis (tissue)						
	Time after injection (min), DUR					
	5		30		60	
	MH134	FM3A	MH134	FM3A	MH134	FM3A
Acid soluble	1.42 ± 0.27	1.15 ± 0.21	1.41 ± 0.07	1.20 ± 0.13	1.04 ± 0.13	0.85 ± 0.15
Lipids (A)	0.05 ± 0.03	0.05 ± 0.03	0.14 ± 0.02	0.13 ± 0.05	0.17 ± 0.06	0.15 ± 0.04
Alkaline- (B)	0.02 ± 0.00	0.02 ± 0.00	0.05 ± 0.01	0.03 ± 0.00	0.07 ± 0.01	0.05 ± 0.00
Acid- (C)	0.02 ± 0.00	0.02 ± 0.00	0.05 ± 0.03	0.04 ± 0.01	0.07 ± 0.02	0.05 ± 0.02
Proteins (D)	0.09 ± 0.02	0.08 ± 0.01	0.41 ± 0.11	0.32 ± 0.07	0.63 ± 0.09	0.48 ± 0.05
(total) (E)	1.60	1.32	2.06	1.72	1.98	1.58
A + B + C + D	0.18	0.17	0.65	0.52	0.94	0.73
(A + B + C + D)/E	11.3%	12.9%	31.6%	30.2%	47.5%	46.2%
D/(A + B + C + D)	50.0%	47.1%	63.1%	61.5%	67.0%	65.8%

Values are mean ± s.d. Value less than 0.0049 = s.d. 0.00. n = 5 each. Alkaline = alkaline-labile fraction containing RNA hydrolysates; Acid = acid-labile fraction containing DNA hydrolysates.

visual contrast of MH134/FM3A was highest in the ^{18}F-FDG macroautoradiogram.

Microautoradiography confirmed that the dense areas of ^{14}C-Met macroautoradiograms consisted of viable cancer cells (Fig. 2A, B). The grain density in a prenecrotic or necrobiotic tumor cell region enclosed within 30–40 μm from focal necrotic cell debris was lower than that in viable cancer cells (Fig. 2C, D). Macrophages and young granulation tissues had lower grain densities (Fig. 2E, F), while extensive necrosis demonstrated the lowest density. Grain distribution of the ^{18}F-FDG macroautoradiogram in the present study confirmed our previous results (*11,12*), demonstrating that marked dense areas were produced by macrophages and young granulation tissues while the relatively lower homogeneous dense areas represented viable cancer cell layers, and grain-free or areas of few grains marked extensive necrotic tissues. Finally, the markedly dense spots were prenecrotic cells embedded in focal necrotic areas.

The film-response curve of ^{14}C is illustrated in Figure 3. The response pattern was similar to that previously reported for ^{18}F (*12*). This result indicates that the profile of both autoradiograms can be compared visually although the optimum exposure time was different.

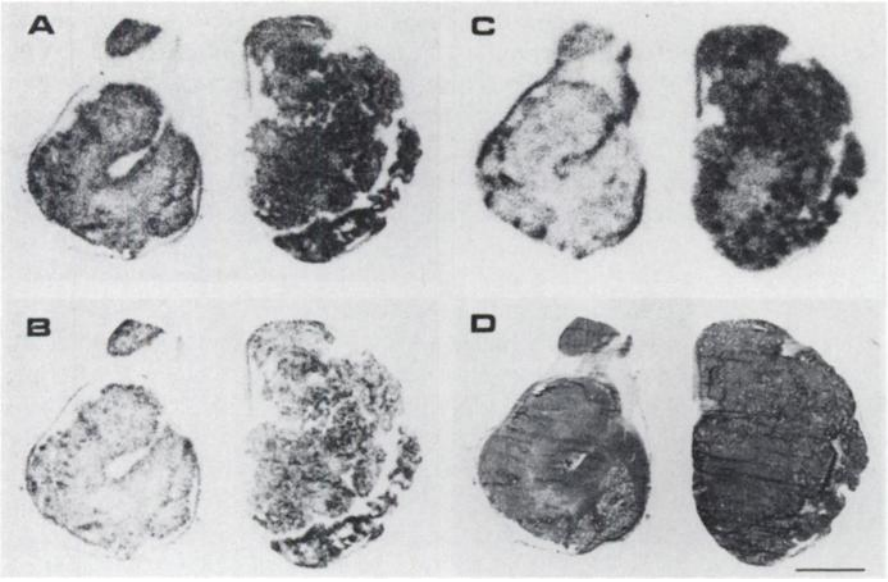

FIGURE 1. A combination of double-tracer macroautoradiograms and microscopy. Images of ^{14}C-Met-whole (A) and -APF bound (B), and ^{18}F-FDG (C) distribution, and a photomicrogram of a specimen (D) used for production of autoradiograms. Left: FM3A tumor; right: MH134 tumor. Scale bar: 2 mm.

Time Course and Tissue Distribution

The uptake of ^{14}C-Met by MH134 and FM3A tumors, muscle and blood were analyzed serially in the first 120 min following injection of ^{14}C-Met (Fig. 4). Carbon-14-Met-whole uptake by MH134 tumors increased rapidly to reach a peak at 30 min, before decreasing. For FM3A, the whole uptake increased for 30 min after injection, then decreased at a rate slower than MH134. The uptake by MH134 was 1.38 ($p < 0.05$), 1.34 ($p < 0.05$) and 1.24 (NS) folds higher than that by FM3A at 30, 60 and 120 min after injection, respectively. On the other hand, ^{14}C-Met-APF bound uptake by MH134 increased at a slower rate reaching a peak at 60 min, before gradually decreasing (Fig. 4). The uptake by FM3A also increased gradually to a peak level at 60 min but plateaued thereafter at 120 min. Carbon-14-Met incorporation into proteins, lipids, RNA and DNA and the degradation were slower in FM3A than in MH134 (Fig. 4, Table 1). Carbon-14-Met-APF bound uptake by MH134 was 1.48 ($p < 0.05$), 1.37 ($p < 0.01$) and 1.05 (NS) and folds higher than that of FM3A at 30, 60 and 120 min after injection, respectively. MH134/FM3A uptake ratios decreased with time. The percentage of ^{14}C-Met-APF bound-to-whole uptake in the whole tumor tissue was increased with time in both tumors (Table 2). In contrast to the

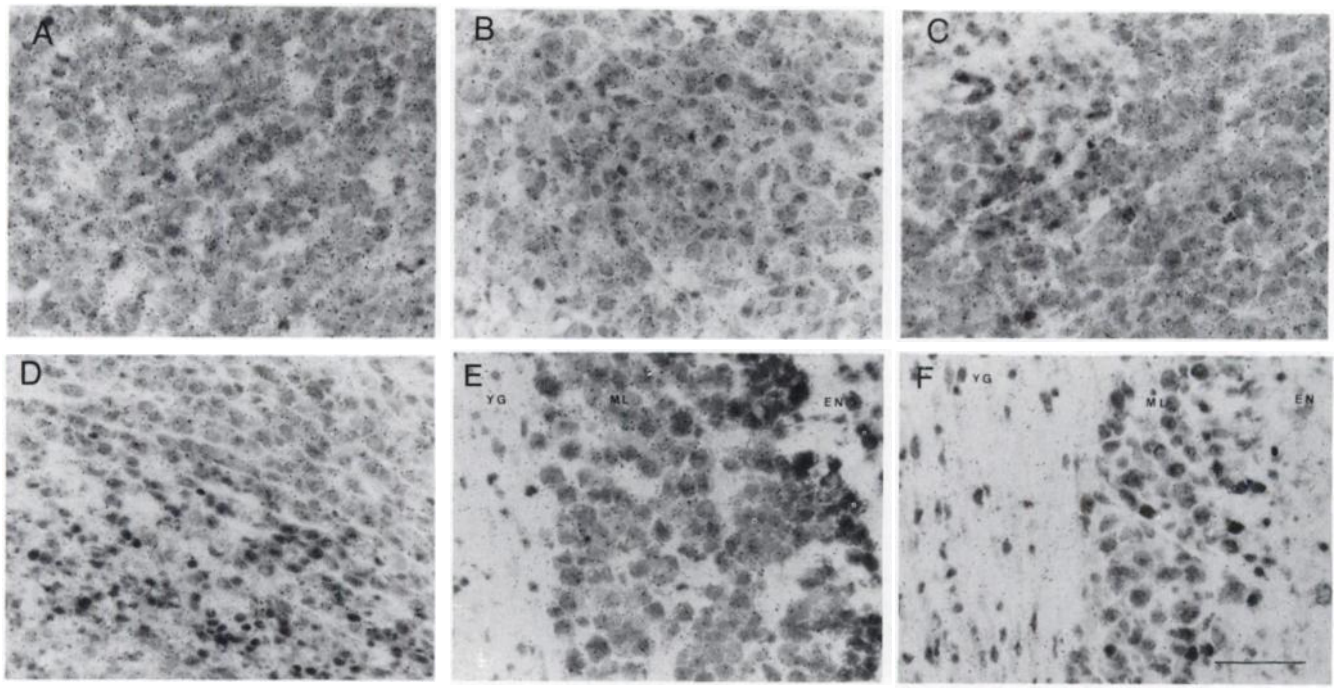

FIGURE 2. Typical microautoradiograms of ^{14}C-Met in tumor tissues. A and B: viable cancer cells; C and D: focal necrotic area (cell debris with surrounding prenecrotic cells) and viable cancer cells (outside prenecrotic cell area); E and F: macrophage layer (ML) and young granulation tissue (YG) at marginal area of extensive necrosis (EN). A, C and E: MH134. B, D and F: FM3A. Bar: 50 μm.

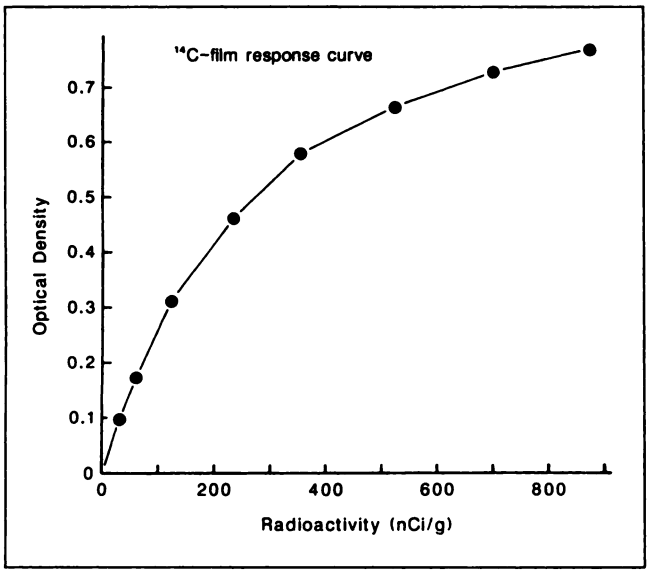

FIGURE 3. Response curve of macroautoradiographic film to ^{14}C. Twelve day exposure.

results of tumor tissues, the uptake by muscles and blood radioactivity level decreased rapidly reaching a plateau at 15 min after injection.

Standard Curves for ^{14}C-Met Microautoradiography

A high linear correlation was demonstrated between the number of silver grains and ^{14}C radioactivity ($y = 0.15x + 2.41$, $r = 0.998$, $p < 0.001$) (Fig. 5). A microautoradiographic study was performed within the confirmed range of linearity. Silver grains were seen in all radioactive tumor sections, while no grains in the control sections were observed. These results exclude a possible positive chemogram.

Time Course of the Uptake of ^{14}C-Met at the Cellular Level

Silver grain density was examined using microautoradiograms of ^{14}C-Met-whole and -APF bound in various cellular elements of MH134 and FM3A tumor tissues. Several variable silver grain densities were histologically identified in different tumor tissue components including: (a) a layer of viable cancer cells found at least 50 μm from necrotic region; (b) a layer of macrophages at outer margin of extensive tumor necrosis; (c) young granulation tissue demarcating intact host tissue; (d) extensive necrosis; (e) focal necrotic cell debris; and (f) regions of prenecrotic cells within 30 μm from focal necrotic cell debris.

Analysis of ^{14}C-Met-whole uptake by MH134 and FM3A demonstrated that the maximum uptake was achieved by viable cancer cells, increasing rapidly to a peak value at 30 min after injection, followed by a gradual decline (Fig. 6A, B). The uptake by MH134 viable cancer cells was 1.55 and 1.44 folds higher than FM3A cancer cells at 30 and 60 min after injection. In contrast, the uptake by young granulation tissue was almost identical in both tumors. The uptake pattern of granulation tissue was similar to that of viable cancer cells, although the uptake level was lower. Prenecrotic cells, macrophages, focal necrotic cell debris and extensive necrotic areas in both tumor types had low uptake of a similar pattern, reaching a peak at 15 min after injection. These tissue components had no proliferating cellular elements. The peak uptake of these elements appeared earlier than that observed in other components with proliferating elements (viable cancer cells and young granulation tissue).

Analysis of ^{14}C-Met-APF bound uptake indicated that viable cancer cells had the highest uptake, followed by granulation tissue, while the uptake by prenecrotic cells, macrophages, focal necrotic cell debris, and extensive necrotic areas was low in both tumors (Fig. 6C, D). Furthermore, the uptake by MH134 viable cancer cells reached a plateau at 45 min after injection while that of the same cells in FM3A tumor continued to increase until 60 min after injection. Thus, ^{14}C-Met incorporation into proteins, lipids, RNA and DNA in viable cancer cells was slower in FM3A than in MH134. The uptake by granulation tissue was almost the same in both tumors showing a gradual increase to a steady level at a later stage.

Comparison of ^{14}C-Met-whole tumor uptake and -APF bound uptake by viable cancer cells indicated that the fraction of percent of bound as part of the whole uptake increased with time in both tumors (Table 2). These values obtained by viable cancer cells were significantly higher than those obtained by whole tumor tissue distribution study described above (Table 2). Because whole tumor tissues and sections included non-neoplastic cellular elements which APF bound uptake was lower. In a separate study using mouse macrophage, monoclonal antibody, macrophages and necrotic tissue accounted for 29.95 and 9.58%, respectively, of the cellular mass of a section of MH134.

DISCUSSION

This study demonstrated that the uptake and clearance of ^{14}C-Met by the whole tumor is faster (peak = 30 min)

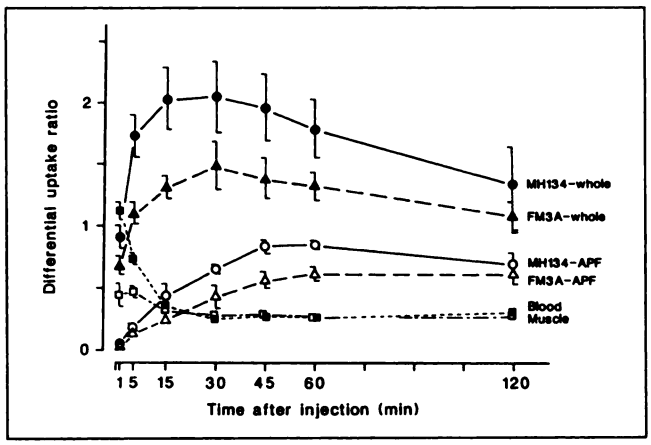

FIGURE 4. Time-course curves for ^{14}C-Met uptake by MH134 and FM3A tumors, muscles and blood levels. Whole = ^{14}C-Met-whole uptake by tumor and APF = ^{14}C-Met-APF bound uptake after extraction.

TABLE 2
Percentage of ^{14}C-Met-APF Bound to Whole Uptake

	A. Whole tumor tissue						
	Time after injection (min)						
	1	5	15	30	45	60	120
MH134	4.8 ± 3.5	10.4 ± 1.8	21.4 ± 5.5	31.4 ± 5.5	42.4 ± 2.8	47.3 ± 5.3	52.0 ± 8.3
FM3A	4.4 ± 3.1	13.5 ± 2.9	18.8 ± 1.5	29.4 ± 3.0	41.6 ± 5.4	46.2 ± 4.6	61.2 ± 12.1

	B. Viable cancer cells in tissue section (microautoradiography, n = 4 each)						
	Time after injection (min)						
	1	5	15	30	45	60	120
MH134	19.1 ± 6.6	25.9 ± 8.1	38.4 ± 7.3	51.0 ± 3.8	66.4 ± 3.7	74.0 ± 10.1	—
FM3A	25.5 ± 14.9	32.6 ± 9.9	48.4 ± 7.9	60.9 ± 5.6	74.2 ± 8.2	80.9 ± 7.8	—

Values are mean ± s.d. Tissue distribution study, n = 4 each.

than that of ^{18}F-FDG (peak = 60 min) (*12*). The methionine uptake profile was consistent with several clinical studies with ^{11}C-Met (*3,16*). Our results indicated that tumor ^{14}C-Met uptake was largely achieved by viable cancer cells. However, ^{14}C-Met-whole uptake did not parallel that of ^{14}C-Met-APF bound uptake, and the incorporation ratio of tracer into proteins, lipids, RNA and DNA increased with time. Significant amounts of free ^{14}C-Met and its metabolites pooled inside tumor tissue. Therefore, the time-related increments in ^{14}C-Met-APF bound uptake is probably due to incorporation of cellularly pooled free ^{14}C-Met/metabolites into macromolecular materials.

The method used in the present study to extract diffusible radioactive metabolites was based on protein precipitation by ethanol (*17*) and on a histological fixation process using EtOH/AcOH as a fixative. Histological fixation is effected by protein degeneration and substitution of cytosol by fixatives. All proteins, except prolamine, are insoluble in alcohol concentrations in excess of 40–50% (*17*). In addition, fixed proteins treated by fixative solution probably become denatured and become irreversibly insoluble and macromolecular materials can not be extracted across cell membranes. Most of lipids are not soluble in ethanol. Thus, the residual radioactivity after extraction/fixation is due to labeled proteins, lipids, RNA and DNA. This method is time-consuming and is not suitable for fractionation analysis using short lived isotopes but, nevertheless, it offers easy preparation of a large number of samples within a short period of time. EtOH/AcOH acted as a fixative in autoradiography because no chemogram was observed by these chemicals.

Our results demonstrated that similar grain numbers in the time course of both ^{14}C-Met-whole and -APF bound study was detected in young granulation tissue of both MH134 and FM3A tumors. This suggests that amino acid demand of peripheral young granulation tissue of tumors of a similar age, in the same host, are highly regulated by the host immune system, independent of differences in tumor type. This property has also been reported recently by Kubota et al. (*12*) in the ^{18}F-FDG uptake study. Carbon-14-Met-APF bound uptake by macrophages showed a very slow incrementing pattern, probably reflecting incorporation of a methyl group from methionine into neutral lipids of monocyte/macrophage (*18*). A recent study from our laboratory has demonstrated that ^{18}F-FDG accumulates in prenecrotic cells (*19*). A similar observation was also seen in the ^{14}C-Met study, the accumulation was, however, not noticeable because of a dominant ^{14}C-Met uptake by viable cancer cells.

The uptake of ^{14}C-Met 60 min after injection in the present study was compared with that of ^{18}F-FDG uptake reported previously in a study from our laboratory (*19*) using the same tumor model and experimental conditions

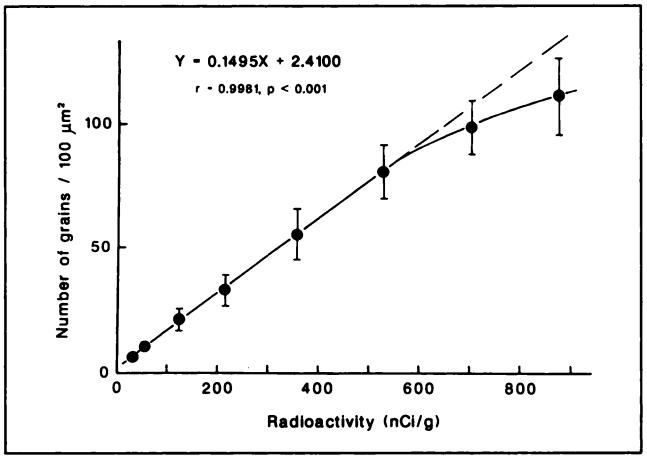

FIGURE 5. A standard curve describing the relationship between silver grain number and ^{14}C radioactivity in microautoradiography.

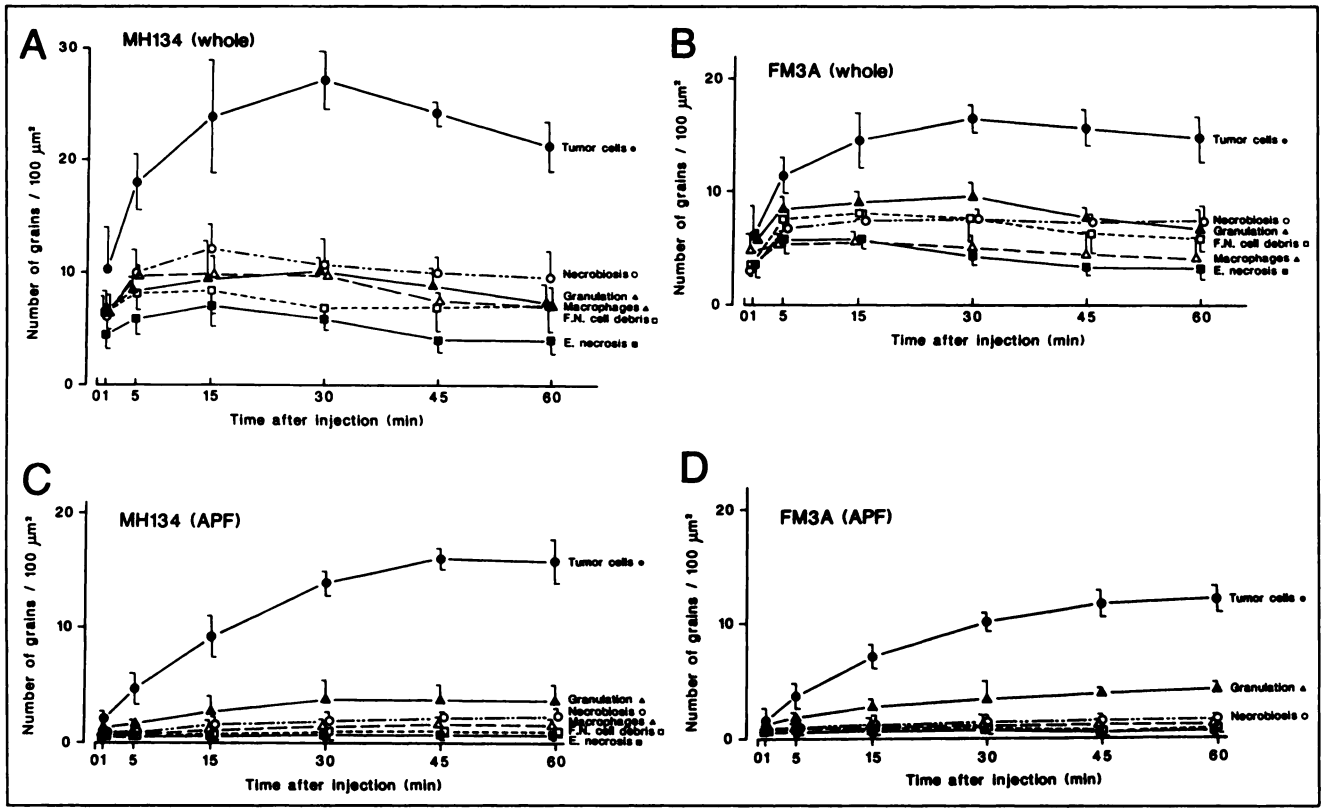

FIGURE 6. ^{14}C-Met-whole and -APF bound uptake in intratumoral components of tumor tissues determined by microautoradiographic silver grain counting. ^{14}C-Met-whole uptake by MH134 (A) and FM3A (B); ^{14}C-Met-APF bound uptake by MH134 (C) and FM3A (D).

(Fig. 7). Such comparison points to the existence of different tumor tissue uptake profiles of the two tracers. Carbon-14-Met-whole uptake by viable cancer cells was high while that by other components was relatively low. Carbon-14-Met reflects the presence/extension of viable cancer cells. Changes in intratumoral components, such as activated macrophages and increased prenecrotic and necrotic cells, may not significantly influence ^{14}C-Met uptake. Therefore, ^{14}C-Met may be suitable for evaluation of cancer treatment. For example, in PET studies of lung cancer, ^{11}C-Met uptake is a good predictor of recurrence after radiotherapy (*20,21*), while ^{18}F-FDG uptake produced the same response in recurrence and no-recurrence group (*22*). In contrast, major tissue components showed a different level of ^{18}F-FDG uptake (Fig. 7). This may explain why visual impression of tumor tissue heterogeneity was higher in ^{18}F-FDG than in ^{14}C-Met as shown in macroautoradiogram (Fig. 2).

As described previously, ^{18}F-FDG uptake in the whole tumor is accentuated by the tumor-associated macrophages and granulation tissues (*12*). Fluorine-18-FDG reflects tumor-host immune system reaction. For treatment evaluation using ^{18}F-FDG, consideration should be given for the presence of an activated immune response and extension of prenecrotic cells (*19*) through which active and passive ^{18}F-FDG uptake may contribute to the activity seen in PET images, particularly in the early period following commencement of treatment (*23,24*). On the other hand, ^{18}F-FDG may represent an excellent tracer to compare tumors of different growth rates prior to the initiation of treatment. The distribution of ^{18}F-FDG, ^{14}C-Met and ^{3}H-Thd in different tissues is summarized in Table 3. Comparison of rapid-to-slow growing tumors showed that MH134/FM3A ratio of ^{18}F-FDG uptake was high while the ratio of ^{14}C-Met and ^{3}H-Thd uptake was lower and similar. Using microautoradiographic grain counts, we have previously demonstrated that MH134/FM3A ratio of de novo DNA synthesis 60 min after injection was 1.84 (*19*). This value is similar to that of ^{18}F-FDG uptake in whole tissue reported in the present experiment (1.75). PET studies have demonstrated that ^{18}F-FDG uptake of head and neck tumors correlates well with the percentage of proliferating cells (*25*). Thus, ^{18}F-FDG may be an ideal tracer for evaluating differences among tumors.

On the other hand, MH134/FM3A ratio of ^{14}C-Met and ^{3}H-Thd uptake ranged from 1.20 to 1.27. It is understood that thymidine uptake in whole tumors does not directly represent de novo DNA synthesis since thymidine is rapidly degraded in vivo and the distribution of metabolites contributes to such activity (*26,27*). Similarly, ^{14}C-Met uptake in the tumor also does not represent protein synthesis and significant amount of labeled metabolites exists in the tissue. A low MH134/FM3A ratio, therefore, suggests that the use of these tracers for comparing tumors of different growth rates may not be discriminatory. In this regard, ^{11}C-Met-PET images of the brain tumor offer a better as-

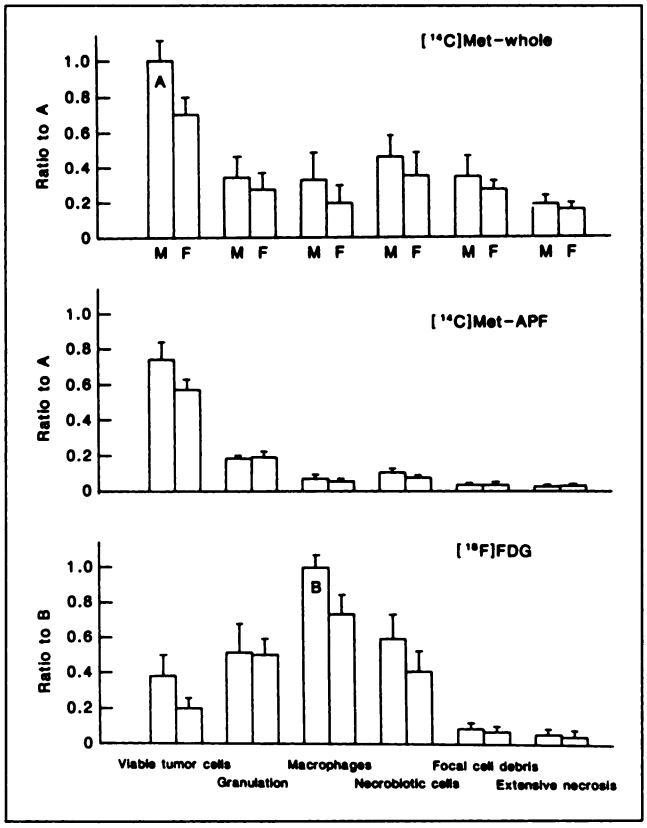

FIGURE 7. Comparison of intratumoral cellular uptake of ^{14}C-Met and ^{18}F-FDG 1 hr after injection. Grain numbers were expressed in values relative to the highest value for each tracer (A for ^{14}C-Met and B for ^{18}F-FDG). M: MH134 tumor; F: FM3A tumor.

sessment of the extent of cerebral glioma rather than evaluating the stage of malignancy (*28–30*). On the other hand, Miyazawa et al. (*31*) recently reported that ^{11}C-Met uptake by lung tumors correlated well with the proliferative cell fraction of the tumor as measured by flow cytometry. However, studies from our laboratory (*5*) indicate that ^{18}F-FDG discriminates between malignant and benign tumors better than ^{11}C-Met.

We believe that the use of each tracer in tumor imaging has certain inherent flaws. If the targeted tumor consists of massive macrophages/immuno-activated cells with few highly proliferating neoplastic cells, ^{11}C-Met uptake may be lower than that of ^{18}F-FDG. Such tumors may give a false negative diagnosis if examined by Met-PET. On the other hand, if the targeted tumor is composed of activated macrophages and prenecrotic cells as a result of treatment, ^{18}F-FDG uptake may be high in spite of a lack of growing malignant cells. Such tumors may lead to a false positive diagnosis if examined by FDG-PET. Thus, the selection of a suitable tracer depends on the type of tumor and aim of the test as each tracer has unique uptake properties. Fortunately, beneficial and weak points of ^{18}F-FDG and ^{11}C-Met are inconsistent. We believe that metabolic information from methionine and thymidine could be complementary to FDG findings.

CONCLUSIONS

In two mouse malignant tumor models with different growth rates, we have shown the following: (1) ^{14}C-Met and ^{18}F-FDG had different distribution patterns in tumor tissue components; (2) the uptake and clearance by whole tumors were faster in ^{14}C-Met than in ^{18}F-FDG; (3) tumor ^{14}C-Met uptake was largely achieved by viable cancer cells. The uptake by macrophages and granulation tissues was low; (4) ^{14}C-Met is a tracer which represents extension/presence of viable cancer cells; ability for evaluation/comparison of tumors of different proliferative activity is inferior to ^{18}F-FDG; ^{14}C-Met is better suited for treatment evaluation of individual tumors; and (5) ^{18}F-FDG reflects tumor-host immune system reaction; It may provide an excellent assessment of pre-treatment tumor proliferative activity.

ACKNOWLEDGMENTS

The authors thank Dr. Prantika Som, Brookhaven National Laboratory, Dr. Zvi H. Oster, State University of New York at Stony Brook and Dr. Kiichi Ishiwata, Tokyo Metropolitan Institute of Gerontology, for advice. We thank Dr. Tatsuo Ido, the staffs of the Cyclotron and Radioisotope Center and Dr. Hiroshi Fukuda, Institute for Aging, Development and Cancer, Tohoku University, for their cooperation and Mr. Y. Sugawara for pho-

TABLE 3
Uptake of ^{18}F-FDG, ^{14}C-Met and ^{3}H-Thd in Triple-Tracer Tissue Distribution Study

Tracer	Time (min)	Differential uptake ratio				
		Blood	Muscle	MH134	FM3A	MH134/FM3A
^{18}F-FDG	30	0.31 ± 0.05	0.34 ± 0.04	2.94 ± 0.16	1.70 ± 0.22	1.73
	60	0.23 ± 0.03	0.37 ± 0.15	3.28 ± 0.40	1.87 ± 0.05	1.75
^{14}C-Met	30	0.54 ± 0.04	0.43 ± 0.05	2.74 ± 0.45	2.26 ± 0.15	1.21
	60	0.49 ± 0.04	0.37 ± 0.03	2.56 ± 0.47	2.10 ± 0.38	1.20
^{3}H-Thd	30	0.50 ± 0.03	0.46 ± 0.04	2.01 ± 0.39	1.58 ± 0.11	1.27
	60	0.49 ± 0.02	0.46 ± 0.03	1.88 ± 0.26	1.50 ± 0.22	1.25

Values are mean ± s.d. n = 5 each time.

tography. We also thank the staff at Word-Medex for their assistance in editing the manuscript. This work was supported by grants-in-aid (04557047 and 06454320) from the Ministry of Education, Science and Culture, Japan.

REFERENCES

1. Som P, Atkins HL, Bandoypadhyay D, et al. A fluorinated glucose analog, 2-fluoro-2-deoxy-D-glucose (F-18): nontoxic tracer for rapid tumor detection. *J Nucl Med* 1980;21:670–675.
2. Larson SM, Weiden PL, Grunbaum Z, et al. Positron imaging feasibility studies. II. Characteristics of 2-deoxyglucose uptake in rodent and canine neoplasms: concise communication. *J Nucl Med* 1981;22:875–879.
3. Kubota K, Matsuzawa T, Ito M, et al. Lung tumor imaging by positron emission tomography using C-11-L-methionine. *J Nucl Med* 1985;26:37–42.
4. Minn H, Paul R, Ahonen A. Evaluation of treatment response to radiotherapy in head and neck cancer with fluorine-18 fluorodeoxyglucose. *J Nucl Med* 1988;29:1521–1525.
5. Kubota K, Matsuzawa T, Fujiwara T, et al. Differential diagnosis of lung tumor with positron emission tomography: a prospective study. *J Nucl Med* 1990;31:1927–1933.
6. Leskinen-Kallio S, Nagren K, Lehikoinen P, et al. Carbon-11-methionine and PET as an effective method to image head and neck cancer. *J Nucl Med* 1992;33:691–695.
7. Kubota K, Yamada K, Fukuda H, et al. Tumor detection with carbon-11-labelled amino acids. *Eur J Nucl Med* 1984;9:136–140.
8. Ishiwata K, Vaalburg W, Elsinga PH, Paans AMJ, Woldring MG. Comparison of L-1-^{11}C-methionine and L-methyl-^{11}C-methionine for measuring in vivo protein synthesis rates with PET. *J Nucl Med* 1988;29:1419–1427.
9. Planas AM, Prenant C, Mazoyer BM, Comar D, Di Giamberardino L. Regional cerebral L-^{14}C-methyl-methionine incorporation into proteins: evidence for methionine recycling in the rat brain. *J Cereb Blood Flow Metab* 1992;12:603–612.
10. Ishiwata K, Kubota K, Murakami M, Kubota R, Sasaki T, Ishii S, Senda M. Re-evaluation of amino acid PET studies: can the protein synthesis rates in brain and tumor tissues be measured in vivo? *J Nucl Med* 1993;34:1936–1943.
11. Kubota R, Yamada S, Kubota K, Ishiwata K, Tamahashi N, Ido T. Intratumoral distribution of fluorine-18-fluoro-deoxyglucose in vivo: high accumulation in macrophages and granulation tissues studied by microautoradiography. *J Nucl Med* 1992;33:1972–1980.
12. Kubota R, Kubota K, Yamada S, Tada M, Ido T, Tamahashi N. Microautoradiographic study for the differentiation of intratumoral macrophages, granulation tissues and cancer cells by the dynamics of fluorine-18-fluorodeoxyglucose uptake. *J Nucl Med* 1994;35:104–112.
13. Kubota K, Ishiwata K, Kubota R, et al. Tracer feasibility for monitoring of tumor radiotherapy: a quadruple-tracer study with ^{18}F-FDG or ^{18}F-FdUrd, ^{14}C-Met, ^{3}H-Thd and ^{67}Ga. *J Nucl Med* 1991;32:2118–2123.
14. Kubota K, Matsuzawa T, Takahashi T, et al. Rapid and sensitive response of carbon-11-L-methionine tumor uptake to irradiation. *J Nucl Med* 1989; 30:2012–2016.
15. Ishiwata K, Kubota K, Murakami M, Kubota R, Senda M. A comparative study on protein incorporation of L-methyl-^{3}H-methionine, L-1-^{14}C-leucine and L-2-^{18}F-fluorotyrosine in tumor bearing mice. *Nucl Med Biol* 1993;20: 895–899.
16. Leskinen-Kallio S, Ruotsalainen U, Nagren K, Teras M, Joensuu H. Uptake of carbon-11-methionine and fluorodeoxyglucose in non-Hodgkin's lymphoma: a PET study. *J Nucl Med* 1991;32:1211–1218.
17. Cohn EJ, Strong LE, Hughes WL Jr, Mulford DJ, Ashworth JN, Melin M, Taylor HL. Preparation and properties of serum and plasma proteins. IV. A system for the separation into fractions of the protein and lipoprotein components of biological tissues and fluids. *J Am Chem Soc* 1946;68:459–475.
18. Bougnoux P, Bonvini E, Stevenson HC, Markey S, Zatz M, Hoffman T. Identification of Ubiquinone-50 as the major methylated nonpolar lipid in human monocytes. *J Biol Chem* 1983;258:4339–4344.
19. Kubota R, Kubota K, Yamada S, Tada M, Ido T, Tamahashi N. Active and passive mechanisms of fluorine-18-fluorodeoxyglucose uptake by proliferating and prenecrotic cancer cells in vivo: a microautoradiographic study. *J Nucl Med* 1994;35:1067–1075.
20. Kubota K, Yamada S, Ishiwata K, et al. PET for treatment evaluation and recurrence detection compared to CT in long term follow-up cases of lung cancer. *Clin Nucl Med* 1992;17:877–881.
21. Kubota K, Yamada S, Ishiwata K, et al. Evaluation of the treatment response of lung cancer with PET and L-methyl-^{11}C-methionine: a preliminary study. *Eur J Nucl Med* 1993;20:495–501.
22. Ichiya Y, Kuwabara Y, Otsuka M, et al. Assessment of response to cancer therapy using fluorine-18- fluoro-deoxyglucose and positron emission tomography. *J Nucl Med* 1991;32:1655–1660.
23. Haberkorn U, Strauss LG, Dimitrakopoulou A, et al. PET studies of fluorodeoxyglucose metabolism in patients with recurrent colorectal tumors receiving radiotherapy. *J Nucl Med* 1991;32:1485–1490.
24. Engenhart R, Kimming BN, Strauss LG, et al. Therapy monitoring of presacral recurrences after high-dose irradiation: value of PET, CT, CEA and pain score. *Strahlenther Onkol* 1992;168:203–212.
25. Minn H, Joensuu H, Ahonen A, Klemi P. Fluorodeoxyglucose imaging: a method to assess the proliferative activity of human cancer in vivo. *Cancer* 1988;61:1776–1781.
26. Cleaver JE. Thymidine metabolism and cell kinetics. In: Neuberger A and Tatum EL, eds. *Frontiers of Biology 6*, Amsterdam: North-Holland Pub. Co.; 1967:15–69.
27. Shields AF, Lim K, Grierson J, Link J, Krohn KA. Utilization of labeled thymidine in DNA synthesis: studies for PET. *J Nucl Med* 1990;31:337–342.
28. Mosskin M, von Holst H, Bergstrom M, et al. Positron emission tomography with ^{11}C-methionine and computed tomography of intracranial tumors compared with histopathologic examination of multiple biopsies. *Acta Radiol* 1987;28:673–681.
29. Ogawa T, Kanno I, Shishido F, et al. Clinical value of PET with ^{18}F-fluorodeoxyglucose and L-methyl-^{11}C-methionine for diagnosis of recurrent brain tumor and radiation injury. *Acta Radiol* 1991;32:197–202.
30. Ogawa T, Shishido F, Kanno I, et al. Cerebral glioma: evaluation with methionine PET. *Radiology* 1993;186:45–53.
31. Miyazawa H, Arai T, Iio M, Hara T. PET imaging of non-small-cell lung carcinoma with carbon-11-methionine: relationship between radioactivity uptake and flow-cytometric parameters. *J Nucl Med* 1993;34:1886–1891.